Optical properties of polymeric materials for concentrator photovoltaic systems

R.H. French [a,b,*], J.M. Rodríguez-Parada [a], M.K. Yang [a], R.A. Derryberry [a], N.T. Pfeiffenberger [a]

[a] DuPont Company, Central Research, Exp. Sta., Wilmington, DE 19880, USA
[b] Department of Materials Science & Engineering, 510 White Hall, 2111 Martin Luther King Jr. Drive, Case Western Reserve University, Cleveland, OH 44106-7204, USA

ABSTRACT

As part of our research on materials for concentrator photovoltaics (CPV), we are evaluating the optical properties and solar radiation durability of a number of polymeric materials with potential in CPV applications. For optical materials in imaging or non-imaging optical systems, detailed knowledge of the wavelength-dependent complex index of refraction is important for system design and performance, yet optical properties for many polymeric systems are not available in the literature. Here we report the index of refraction, optical absorbance, haze, and Urbach edge analysis results of various polymers of interest for CPV systems. These values were derived from ellipsometry and from using a VUV-VASE and transmission based absorbance spectroscopy on thick film samples.

Fluoropolymers such as poly(tetrafluoroethylene-co-hexafluoropropylene) (Teflon® FEP), poly(tetrafluoroethylene-co-perfluoropropyl vinyl ether) (Teflon® PFA) and poly(ethylene-co-tetrafluoroethylene) (Teflon® ETFE Film) have desirable optical and physical properties for optical applications in CPV. Ethylene backbone polymers such as polyvinylbutyral (PVB) sheet (e.g., DuPont™ PV5200), and ethylene co-polymers such as poly(ethylene-co-vinyl acetate) (EVA) (e.g., DuPont™ Elvax® PV1400), and poly(ethylene-co-methacrylic acid metal salt) ionomer sheet (e.g., DuPont™ PV5300) have applications as encapsulants in crystalline silicon (c-Si) and other flat plate PV applications. These materials are available with both a wide variety of polymer compositions and additive packages which affect their optical properties such as the UV absorption edge. Even materials such as DuPont's Kapton® polyimide films, which are used behind the PV cell for their electrically insulating properties, have optical requirements, and we have also characterized these materials.

The detailed optical properties of these materials will be useful in the design of the geometrical optics of a CPV system and optimization of the system's optical throughput. This information will also provide insights into the system's optical absorption. This is important, for example in the UV, where this absorption can impact the radiation durability of the materials.

1. Introduction

Concentrating photovoltaic (CPV) systems and their optical materials have come from a wide background of similar optical reduction technologies. For example, they can be closely related to the field of optical lithography [1], which relies greatly on reduction optics of liquids for precise nanoscale patterning. This carries over to the primary optics (those used with 1 sun irradiance) and the secondary optics (those used at multiple sun irradiances) in a CPV system. According to Swanson [2], CPV systems can be divided into low, medium, and high concentrators, as seen in Fig. 1 [2]. Low concentrators employ 1–10 × concentration with no tracking of the sun, and cells made of silicon or thin film. Medium concentrators employ 12–100 × concentration with one- or two-axis tracking of the sun, and cells made of silicon. High concentrators employ 200–2000 × concentration with high precision two-axis tracking of the sun, and multi-junction III–V cells.

For optical materials in imaging or non-imaging optical systems, detailed knowledge of the wavelength-dependent complex index of refraction, $\hat{n}(\lambda) = n(\lambda) + ik(\lambda)$, is important for the optical system's design and performance. The index, n, and the extinction coefficient, k (which is directly related to the optical absorbance $\alpha = 4\pi k/\lambda$), give insights into the system's optical performance. The index of refraction determines reflectance losses at air/polymer,

* Corresponding author at: Department of Materials Science & Engineering, 510 White Hall, 2111 Martin Luther King Jr. Drive, Case Western Reserve University, Cleveland, OH 44106-7204, USA. Tel.: +1 216 368 3655.
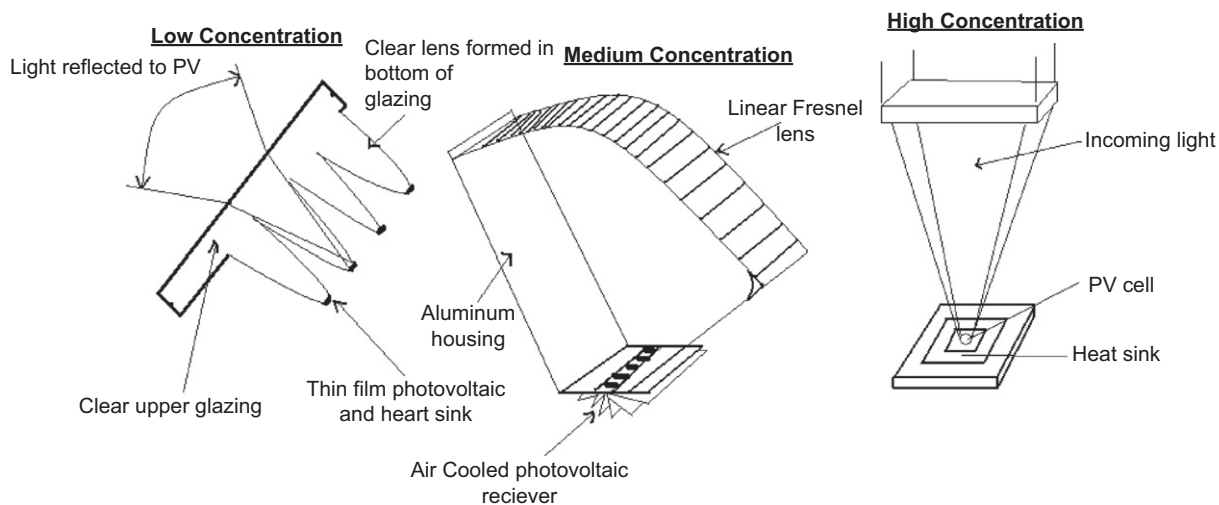E-mail address: roger.french@case.edu (R.H. French).

Fig. 1. Low concentration (left), medium concentration (middle), and high concentration CPV systems (right) [2].

polymer/polymer and polymer/inorganic interfaces, and is important for matching or optimizing the numerical aperture (NA) of the reduction optical system at all points in the optical path. The extinction coefficient is critical to determine optical losses in the system, including the passage of ultraviolet (UV) through the system. The absorption of UV light by the optical materials can also contribute to optical degradation of the materials due to photodarkening and photobleaching and other types of degradative processes and reduced performance over time [3].

CPV is typically non-imaging [4]; therefore, cost-effective materials that do not have perfect optical clarity are still of interest. For optics with short throw lengths (or focal lengths), haze can help homogenize the light. Haze can also be important for optics with long throw lengths, such as primary optics, refractive lenses, and reflective mirrors in which specularity is important. The distinctness of image or DOI [5] is the deviation of the direction of light propagation from the regular direction via scattering during transmission or reflection and can be related to haze. DOI is useful for characterization of the visual appearance of CPV materials.

In addition to the refractive optical materials, many CPV systems utilize mirrors; therefore, materials for multilayer reflectors are also of interest. Metallized fluoropolymers for back side mirrors used in CPV or concentrating solar power optics have reflectance values above 90% after 3.5–4 years of exposure [6]. Their use in concentrated solar power technologies would not be limited if their specularity could be sufficiently improved, for example by reducing the haze which can be associated with scattering and reduced specularity on a reflector [6]. The specularity was determined in both a 25 mrad (milliradian) cone and a 7 mrad cone, and for mirror applications which have long optical path (or "throw" lengths); the tighter 7 mrad specularity measurement is important. CSP tower applications, which typically have long distances from the reflecting mirror surface to the power tower absorbing surface, are an example of this long throw length mirror application.

We have previously studied [7] Teflon® AF, an amorphous perfluoro-2,2-dimethyl-1,3-dioxole/tetrafluoro-ethylene (PDD/TFE) copolymer, which can be used as a photo mask pellicle in IC fabrication. We found that the optical properties of three grades of Teflon® AF varied systematically with the copolymer composition associated with changes in the run lengths of monomer units in the polymer backbone. Teflon® AF has one of the lowest index of refraction ($1.28 < n$ (589.3 nm) < 1.30) and

shortest wavelength optical absorption edge onset (158 nm or 7.85 eV) known for a polymer. We also developed other novel fluoropolymers, such as $-[(CH_2CHF)xC(CF_3)2CH_2]y-$, or $-(CH_2CF_2)x[2,2\text{-}bis(trifluoromethyl)\text{-}4,5\text{-}difluoro\text{-}1, 3\text{-}dioxole]y-$, with optical absorption edges onsets down to 144 nm (or 8.61 eV) [8]. We have also studied amorphous and crystalline silica [9], other oxides [10,11], nitrides [12], and carbon nanotubes [13,14], as well as polystyrene [15] and novel backbone polymers such as the polysilanes [16].

The optical absorption/cm and haze of various polymeric compositions have previously been measured for various fluoropolymers, including perfluoropolyethers (PFPE) [17], fluorinated polyimides [18], polytetrafluoroethylene (PTFE) [19], and other DuPont fluoropolymers [7,8,20]. While the ASTM standard haze measurement is an object dependent value and varies based on sample thickness and bulk crystalinity, since all of the evaluations were performed on the same instrument and in the same orientation, haze can be a useful measurement for rank-ordering the polymer's clarity that arises from bulk and surface scattering. Prior research on the optical properties of polyimides including Kapton®, Upilex®, and polyimide derivatives like TOR and CP were published by Russell al. [21]. There have been also numerous studies on the index of refraction versus wavelength for PTFE [22], polyimides [23,24], polyesters [25], and acrylics [26].

Wallner et al. [27,28] developed a fundamental understanding of the physical relationships between the material structure and solar optical properties, as well as the infrared optical properties, of transparent polymeric materials. Their studies included low- and high-temperature resistant polymer films such as polymethyl methacrylate (PMMA), polyethylene terephthalate (PET), polycarbonate (PC), polyimide (PI), and poly(tetrafluoro-ethylene-co-perfluoroalkylvinyl ether) (PFA) [29]. They have also tested the solar radiation durability of PC, PMMA and PET [30,31].
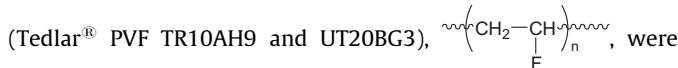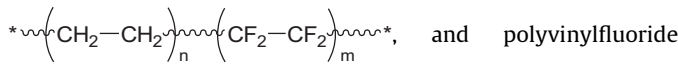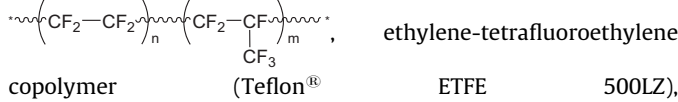
For potential CPV applications, we report the optical properties, including spectral index of refraction, optical absorbance, and haze, of various fluoropolymers, ethylene backbone polymers, and polyimides. The detailed optical properties of these materials will be useful in the design of the geometrical optics of a CPV system and optimization of the system's optical throughput. The information will also provide insights into the system's optical absorption. This is important, for example in the UV region, where this absorption can impact the radiation durability of the materials.
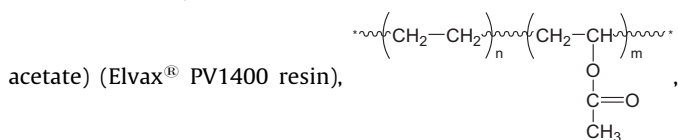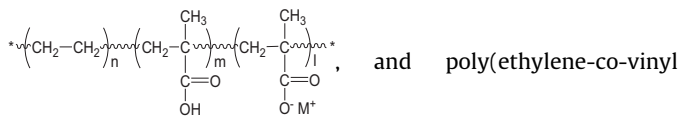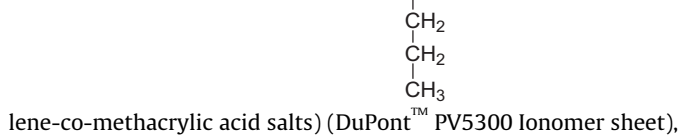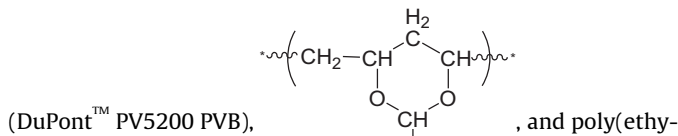
2. Experimental methods

2.1. Materials

The materials we report on here fall into to three families: fluoropolymers, ethylene backbone polymers, and polyimides.

Fluoropolymers (FP): Films of tetrafluoroethylene–hexafluoropropylene copolymer (Teflon® FEP 500A),

$$\sim\!\!\left(CF_2\!-\!CF_2\right)_n\!\!\left(CF_2\!-\!CF\right)_m\sim, \quad \text{CF}_3$$

ethylene-tetrafluoroethylene copolymer (Teflon® ETFE 500LZ),

$$*\!\sim\!\!\left(CH_2\!-\!CH_2\right)_n\!\!\left(CF_2\!-\!CF_2\right)_m\!\sim\!*,$$

and polyvinylfluoride (Tedlar® PVF TR10AH9 and UT20BG3),

$$\sim\!\!\left(CH_2\!-\!CH\right)_n\!\sim, \quad \text{F}$$

were obtained from DuPont Fluoroproducts. The use of these materials in conventional PV modules is well documented [32].

Ethylene backbone polymers (EBP): Polyvinylbutyral (DuPont™ PV5200 PVB), and poly(ethylene-co-methacrylic acid salts) (DuPont™ PV5300 Ionomer sheet), and poly(ethylene-co-vinyl acetate) (Elvax® PV1400 resin), were obtained from DuPont Packaging and Industrial Polymers. Films of different thickness were made by melt pressing.

Polyimides (PI): Kapton® H, Kapton® HN, and Kapton® E were obtained from DuPont Electronic Technologies.
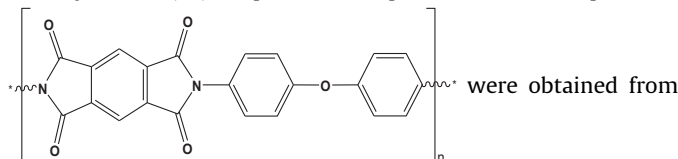
2.2. Spectroscopic Ellipsometry

Variable angle spectroscopic ellipsometry (VASE) [33–35] measurements were performed with a VUV-VASE® VU-302 [36], which has a range from 0.69 to 8.55 eV (1800 to 145 nm), and employs MgF_2 polarizers and analyzers rather than the more common calcite optics. The spectrometer was upgraded from single beam to dual beam for more accurate transmission measurements and better instrument stability. The instrument has a MgF_2 auto-retarder and is fully nitrogen-purged to avoid absorption of VUV light by ambient oxygen and water vapor, which is important at wavelengths below 200 nm. Light from both the deuterium lamp and the xenon lamp pass through a double-chamber Czerny-Turner type monochromator to provide wavelength selection and stray-light rejection. The spot diameter of

light source on the surface of the sample is 2 mm. Computer-controlled slit widths adjust the bandwidth to insure adequate spectral resolution of optical features in the data. These include closely spaced interference oscillations, which arise in very thick films. A photomultiplier tube is utilized for signal detection in the ultraviolet. A stacked Si/InGaAs photodiode detector is used for longer wavelengths. Ellipsometric measurements were conducted using light incident at angles of 65–75° relative to normal on the front surface of the sample, the back of which was roughened with coarse polishing paper. The instrument measures the ellipsometric parameters Ψ and Δ, which are defined by [37]:

$$\tan(\Psi)e^{i\Delta} = \frac{R_P}{R_S} \tag{1}$$

where R_P/R_S is the complex ratio of the p and s-polarized components of the reflected amplitudes. These parameters were analyzed using the Fresnel equations [38] in a computer-based modeling technique, which includes a surface roughness layer to directly determine the optical constants [39,40]. An effective medium approximation (EMA) surface roughness layer was used since the surface roughness of the samples was small. The EMA surface roughness layer was used to model the ellipsometric data and determine the complex optical properties of the polymeric systems in question. Since surface scattering in ellipsometry does not impact the complex optical properties n and k determined, this technique is well established in the literature for optical property determination. VUV-VASE® VU-302 measurements for this experiment were taken from the wavelength range 145–1650 nm at multiple angles of incidence (65–75°). Variable angles improve confidence as light travels different paths through the film.

The ellipsometry data, taken from the film, was fit to determine the polymer film roughness, thickness non-uniformity, and complex refractive index [41]. An optical model was used to describe the film optical constants over the wide spectral range [42].

The film was modeled using initial optical constants from Woollam. A thin EMA surface roughness layer, consisting of 50/50 mix of organic film and void ($n=1$) was used. In the initial stage, a Cauchy dispersion model was used to fit the transparent region of 500–1550 nm. Then, the complete model was minimized by fitting the optical constants on a point-by-point basis over the full spectral range in which the data in each single wavelength is fit separately.

2.3. Optical absorbance and haze

The optical absorbance of free-standing films was determined by the center-mount absorbance method (Fig. 2) using a Cary 5000 UV–Vis–NIR spectrophotometer with a DRA-2500 integrating sphere [43]. The measured value of absorbance was divided
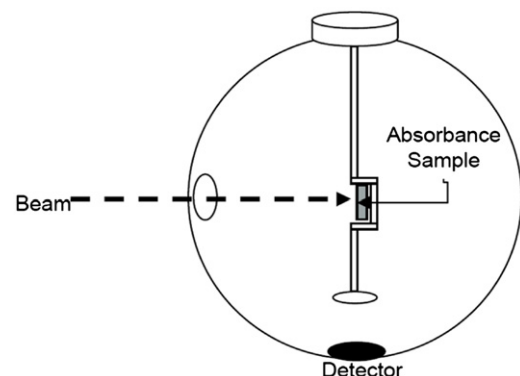

Fig. 2. Center-mount absorbance method.

by the film thickness to obtain a value of optical absorbance per cm (base 10).

For films coated on ultrahigh purity fused silica substrates, once the transmission spectra of the film was determined, the film's optical absorbance per cm (base 10) could be determined by:

$$A/\text{cm} = \frac{\log_{10}\left[T_{substrate}/T_{film}\right]}{t_{film}} \qquad (2)$$

where T is the transmission, t is the thickness of the film, and A/cm is the absorbance per centimeter. Using multiple samples of different film thickness, one can then solve the resulting system of equations and determine the reproducibility and standard deviation of the optical absorbance per centimeter [44].

The calculation of optical absorbance assumes that the film is of homogenous composition and uniform thickness. Therefore, an integrating reflectance accessory is required and the reflectance measured is predominately specular [45]. Transmission-based measurements also require that the film thickness of the sample on the substrate be optimized for the dynamic range of the technique so that the transmittance of the film falls in the range from 3% to 90%. If the transmittance falls much below 1%, the accuracy of the measurement is severely degraded, and erroneous results appear.

Once the extinction coefficient, k, and the base 10 optical absorbance per cm, A/cm, have been determined, the base e optical absorption coefficient, α, can be determined using Eq (3). The absorption coefficient, α, corresponds to the attenuation of the light transmitted through the sample and is calculated on a natural logarithm basis. Since the absorbance per cm, A/cm, is determined from the base 10 logarithm of the optical density given in Eq. (3), a value of $\ln(10)$, or 2.302585, is introduced into Eq. (4). Both k and α are inherent optical properties of the material. On the other hand, absorbance per centimeter is frequently based only on transmission measurements, and thus neglects effects arising from the index mismatch between the film and substrate, thin film interference effects, and film non-uniformity effects.

The fundamental absorption edge spectra have been determined by:

$$\alpha = 4\pi k/\lambda \qquad (3)$$

where α is the optical absorption coefficient (base e), λ is the wavelength of the light source, and k is the extinction coefficient. The relationship between the base e absorption coefficient α and the base 10 absorption coefficient A is given by:

$$A = \frac{\log_{10}(T_1) - \log_{10}(T_2)}{t} = \frac{1}{\ln(10)}\frac{\ln(T_1) - \ln(T_2)}{t} = \frac{1}{\ln(10)}\alpha \qquad (4)$$

where T_1 is the transmission of substrate, T_2 is the transmission of film, and t is the thickness of film as given in Table 1.

The Cary 5000 UV–Vis–NIR spectrophotometer (Varian) is also used for the haze measurement. The instrument utilizes a hemispherical optical measuring system, with an integrating sphere, in
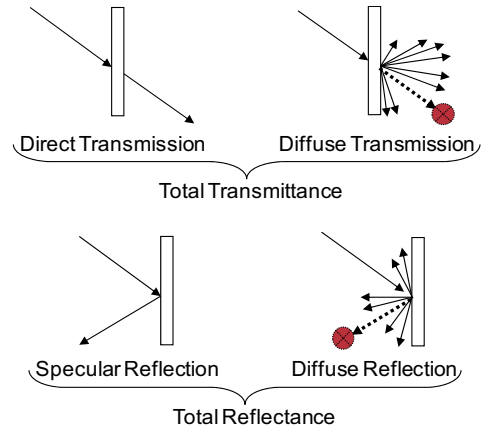

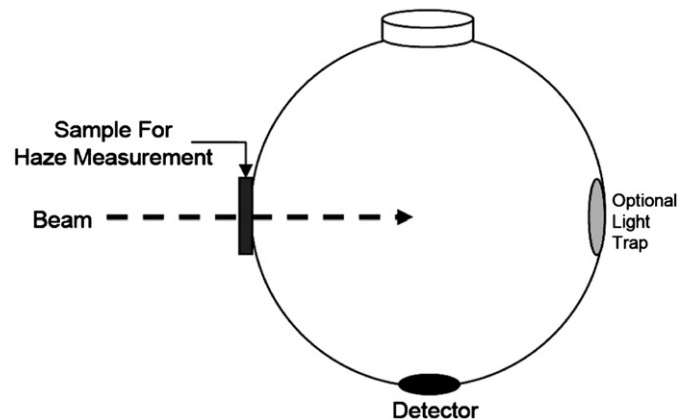Fig. 3. The components of the total transmittance and total reflectance.

Fig. 4. ASTM D 1003 procedure B for haze measurement utilizing unidirectional illumination with diffuse viewing geometry.

which the specimen is placed flush against the sphere port. A unidirectional illumination with diffuse viewing geometry was used. The transmission (total and scattered) and reflectance (diffuse+specular and diffuse only; defined in Fig. 3) were measured using the ASTM D 1003 procedure B (Fig. 4). Eq. (5) was used to calculate the percent haze

$$\text{Haze} = T_d/T_t \times 100 \qquad (5)$$

where T_d is the diffuse transmittance and T_t is the total transmittance.

The above measurements were conducted under the following conditions: The external DRA-2500 was installed into the spectrophotometer and aligned. UV-Vis-NIR spectra were, in general, acquired in the region 200–2500 nm using appropriate baseline correction (zero/baseline for %T and absorbance, zero x standard reference for reflectance, correction for spectral only). Indicative instrumental parameters were as follows: spectral bandwidth (SBW)=4 nm (UV/Vis) or 16 nm (NIR); averaging time=0.4 s; data interval=2 nm; double beam mode using full slit height for %T and absorbance, reduced for %R. A mask over the sample port was used with a reduced slit for the reflectance data, and was in place during baseline and sample collection. A small spot kit (SSK) was used for the center mount absorbance data (not reflectance).

As in all experimental measurements, the accuracy of the measured values is a function of the sample and measurement apparatus. The inherent sensitivity of spectral transmission and absorbance measurements is affected by the optical path length

Table 1
Sample thickness (t) in mils (0.001 in.).

	Tedlar® PVF				
	UT20BG3	TR10AH9	ETFE	FEP	PFA
FP					
t	2	1	5	5	5
EBP	PV1400 EVA	PV5200 PVB		PV5300 Ionomer	
t	15	10		15	
PI	Kapton® H	Kapton® HN		Kapton® E	
t	2	2		2	

of the sample, and the transmission drop that occurs as light transmits through the sample. As the transmission drop decreases, the accuracy of absorbance measurement decreases. A transmission difference of ~0.1% is near the limit of the measurement method.

2.4. Urbach Analysis of Absorption Edges

Urbach edge analysis is a useful way to parametrically characterize a film's optical absorption edge and to distinguish intrinsic and extrinsic contributions to the absorbance [44]. Urbach [46] originally observed that a material's optical absorption for energies below the fundamental optical absorption edge is exponential in nature and can be characterized by the Urbach edge energy (E_0) and the Urbach width (W), which is related to the slope of the Urbach edge (using the nm$\Leftrightarrow$eV conversion, $\lambda(nm) = 1239.8/E$ (eV)).

2.5. Urbach analysis of the absorption coefficient (α) and the absorbance (A)

For Urbach fits to α, either Eq. (6) is used

$$\alpha(E) = H_\alpha \exp\left(\frac{E - E_{0\alpha}}{W_\alpha}\right) \tag{6}$$

Where the absorption coefficient α as a function E is characterized by the Urbach edge energy (E_0) and the Urbach width (W). The intercept $E_{0\alpha}$(energy at which $\alpha = 1$) is the quantity of interest.

For Urbach fits to A, the following equation is used:

$$A(E) = H_A \exp\left(\frac{E - E_{0A}}{W_A}\right) \tag{7}$$

The intercept E_{0A}(energy at which $A = 1$) is the quantity of interest. The relationship between $E_{0\alpha}$ and E_{0A} is obtained as follows:

$$A(E) = H_A \exp\left(\frac{E - E_{0A}}{W_A}\right) = \frac{\alpha}{\ln(10)} = \frac{H_\alpha}{\ln(10)} \exp\left(\frac{E - E_{0\alpha}}{W_\alpha}\right) \tag{8}$$

Note that Urbach actually fits the exponential equations shown above. This is done because the error statistics are known in data space (A and α), not in ln(data) space.

3. Lorentz oscillator modeling

The Lorentz oscillator (LO) [47] is a useful tool for studying the optical behavior of optical materials and for modeling complex optical properties. The optical properties of a Lorentz oscillator model can be solved analytically and represent an exact solution to Maxwell's equations of light for the response of a simple harmonic oscillator to an electromagnetic wave. Using the quantum mechanical form of the Lorentz oscillator, and allowing the construction of models involving multiple oscillators, one can build models and determine their complex optical property responses. Consider the Lorentz oscillator equation for the complex dielectric function (ε) as a function of photon frequency (ω)

$$\hat{\varepsilon}(\omega) = 1 + \frac{4\pi N e^2}{m} \sum_j \frac{f_j}{(\omega_j^2 - \omega^2) - i\Gamma_j \omega} \tag{9}$$

Here Γ_j is oscillator width, ω_j is oscillator frequency, N is electron density, and f_j is the oscillator strength. The plasma frequency, ω_p,
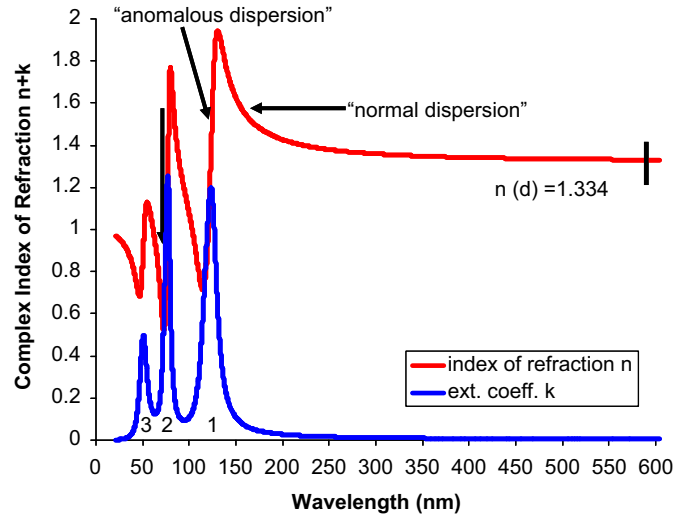

Fig. 5. The refractive index, n, and extinction coefficient, k, of a Lorentz oscillator model normal and anomalous dispersion, using three oscillators. This model mimics the index and dispersion of water in the UV.

is directly related to the electron density N.

$$\omega_p = \frac{4\pi N e^2}{m} \tag{10}$$

In the quantum mechanical Lorentz oscillator model, the oscillator strengths are defined to sum to 1, as shown in Eq. 11.

$$\sum_j f_j = 1 \tag{11}$$

Note that one can calculate the complex refractive index from the dielectric function of the LO using:

$$\varepsilon_1 + i\varepsilon_2 = (n + ik)^2 \tag{12}$$

One can also calculate the absorption coefficient α using Eq. (3).

For a model optical material, we then construct a LO model using three oscillators to represent low, medium, and high energy interatomic bonds in the material, and we adjust the plasma frequency, the oscillator energies, widths, and strengths, to yield a model that has the same spectral refractive index in the UV and visible region as water in this example. Such a model, reproducing water's index, is shown in Fig. 5.

4. Results and discussion

We present results on the spectral index of refraction, the absorbance per centimeter, the haze, and the Urbach edge analysis of the materials of interest. The refractive index (n and k) and transmission intensity of materials of potential interest to CPV were determined over the wavelength range 145–1650 nm.

Through comparison of our optical properties with those reported by Miller [48] of the National Renewable Energy Laboratory (NREL), one can see that each are coming at the optics and optical properties from a different viewpoint. In our case we think of the optical properties of the bulk materials, whereas NREL approaches the problem of the optics from an overall CPV system perspective. Therefore they tend to utilize different metrics such as the use an "absorptance" [49], which is the fraction of light

absorbed by a sample at a specified wavelength

$$\mathcal{T}_\lambda = \frac{I}{I_0} \quad \mathcal{A}_\lambda = \frac{I_0 - I}{I_0} \tag{13}$$

where I_0 is the intensity of the incident light, I is the intensity of the light coming out of the sample, and $\mathcal{T}_\lambda$ and $\mathcal{A}_\lambda$ are transmittance and absorptance, respectively. In these equations, scattering and reflection are considered to be close to zero or otherwise accounted for. The transmittance of a sample is sometimes given as a percentage. Thus the absorptance is dimensionless, and it is more from the "optical system point of view". The absorptance is for transmission of some given thickness of a material, as stated in [48], where $\mathcal{A}_\lambda$ was scaled for 0.5 mm thickness for polymer films to directly compare the optical measurements from different specimens, whereas our optical properties are of materials, which are directly comparable, and are thickness independent.

We report specimen thickness in cm and base e α, cgs (cm gm s units) optical properties, and the absorption coefficient in units of 1/cm. NREL reports (m) and $(m^{-1}$ must be superscript to m.) as the unit of specimen thickness and the absorption coefficient as base e α. We found that the results from these two different and complementary approaches are comparable and in agreement. For example, a similar shape of spectra of the ethylene backbone polymers shown in Fig. 5 in [48] is observed comparing Fig. 11. We also see that the ethylene backbone polymers demonstrate some absorbance of UV light and IR from the optical absorbance A (base 10, 1/cm, Fig. 11) and NREL's optical absorption curves (%, unitless) [48].

The refractive index of quartz is compared with other materials in NREL's studies [48]. We have previously studied the optical properties of amorphous silica (a-SiO$_2$; ultrahigh-purity fused silica) and crystalline silica (c-SiO$_2$; α-quartz) by vacuum ultraviolet spectroscopy and spectroscopic ellipsometry [9]. We found that crystalline SiO_2 has a higher reflectance, index of refraction, and dielectric constant than amorphous SiO_2. The complex index of refraction for both crystalline and amorphous SiO_2 within the energy range from 0.7 to 8 eV (155–1771 nm) agrees very well with previous literature results [50].

4.1. Fluoropolymers (FP)

Fluoropolymers are widely used in the photovoltaic industry because of their chemical and environmental resistance, durability, flexibility, electrical isolation, photostability, and moisture resistance [51]. Fluoropolymers are readily available in film form, which is preferred in photovoltaic applications. The weight of a PV module can be reduced by replacing the front glass sheet with a flexible fluoropolymer front sheet. Based on NREL studies, fluoropolymers such as Teflon® FEP have excellent solar radiation durability, having shown little change in optical properties after 27 years of 1 sun solar exposure [52]. Tedlar® PVF films have been an essential component of photovoltaic back sheets for more than 25 years, and are widely recognized as the industry standard due to its excellent strength, weather resistance, ultraviolet resistance, and moisture barrier properties.

4.1.1. Index of refraction

The index of refraction versus wavelength for the fluoropolymers studied is shown in Fig. 6. Their values at the sodium D-line are also summarized in Table 2. The lower indices of refraction correspond to Teflon® PFA and Teflon® FEP, which are about 76 wt% fluorine. As the weight percent fluorine decreases in fluoropolymers, the index increases. Teflon® ETFE is an approximately alternating copolymer of ethylene and

Fig. 6. Index of refraction, n, determined from ellipsometric data for fluoropolymer films.

Table 2
Index of refraction (n) at D-line (589.3 nm).

FP	Tedlar® PVF UT20BG3	Tedlar® PVF TR10AH9	Teflon® ETFE	Teflon® FEP	Teflon® PFA
n at D-line	1.474	1.478	1.398	1.350	1.343
EBP	PV1400 EVA	PV5200 PVB		PV5300 Ionomer	
n at D-line	1.489	1.480		1.487	
PI	Kapton® H	Kapton® HN		Kapton® E	
n at D-line	1.824	1.817		1.899	

tetrafluoroethylene, which results in a fluorine content of about 59 wt%. Tedlar® PVF has a fluorine content of 41 wt%.

These fluoropolymers exhibit normal dispersion in the visible and UV spectral regions down to wavelengths below 200 nm. Normal dispersion is observed as the wavelength of the light approaches the fundamental absorption edge [44]. Anomalous dispersion arises at wavelengths shorter than the fundamental absorption edge, where the index is seen to decrease with decreasing wavelength. The regions of normal and anomalous dispersion are identified for a Lorentz oscillator model shown in Fig. 5. In addition, the transition from normal to anomalous dispersion is shown in Fig. 6 for Teflon® FEP and PFA, and also in Fig. 13 for the polyimides.

4.1.2. A/cm and haze

The A/cm and haze of the fluoropolymers are shown in Fig. 7 and 8, respectively. The fundamental absorption edge of Teflon® FEP, Teflon® PFA, and Teflon® ETFE is at wavelengths below 200 nm and therefore the A/cm is very low at all solar wavelengths. Tedlar® PVF TR10AH9 film shows an absorption edge below 300 nm, while Tedlar® PVF UT20BG3 film essentially blocks most radiation at wavelengths below 400 nm. Its A/cm at longer wavelengths is still very low and comparable to the other fluoropolymers. Even though all the fluoropolymers studied here are semicrystalline materials, only films of Tedlar® PVF UT20BG3 and Teflon® ETFE exhibit significant haze. Teflon® FEP, Teflon®
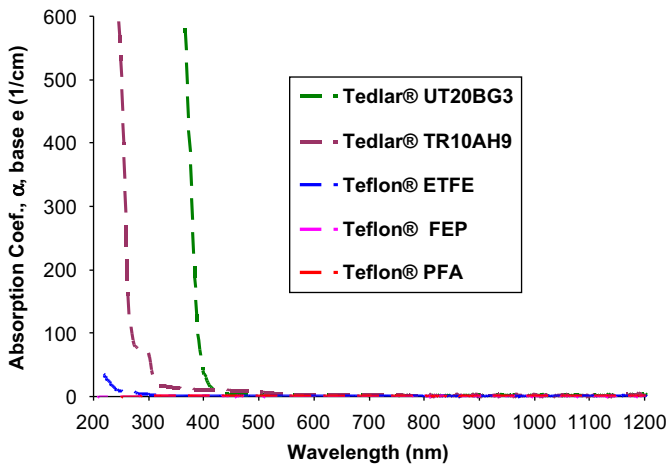
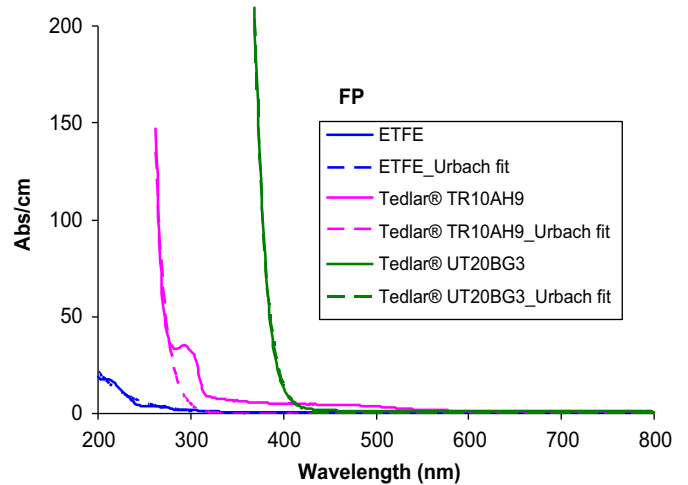**Fig. 7.** Optical absorbance of fluoropolymer films.

Fig. 8. Haze of fluoropolymer films.

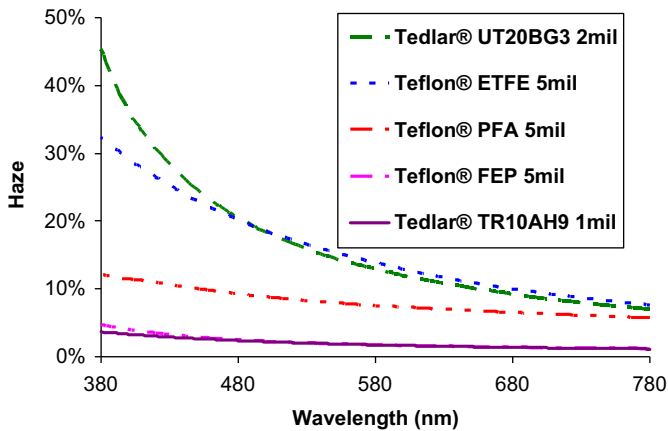**Fig. 9.** Optical absorption edge of Teflon® ETFE and Tedlar® PVF films with their corresponding Urbach edge fits.

Table 3
Urbach edge fit parameters.

Materials	Urbach edge position (nm) from absorbance fits	Urbach edge width (nm) from absorbance fits	Urbach fit range (nm)	Abs offset correction
Tedlar® PVF UT20BG3	454	17	368–800	No
Tedlar® PVF TR10AH9	308	9	262–800	No
Teflon® ETFE	314	37	185–800	Yes
PV1400 EVA	266	10	230–258, 295–800	No
PV5200 PVB	366	29	250–266, 416–800	No
PV5300 Ionomer	346	27	232–268, 393–800	No
Kapton® H	741	47	492–1000	No
Kapton® HN	731	45	494–1000	No
Kapton® E	763	56	462–1000	No

PFA, and Tedlar® PVF TR10AH9 films are very clear and show much less haze than the UV-opaque Tedlar® grade. While haze measurements are relatively independent of wavelength below the fundamental absorption edge, these materials show some degree of bulk haze given long enough optical path lengths.

4.1.3. Urbach edge analysis

In the Urbach analysis of the absorbance (*A*), as the weight percent of fluorine decreases in the polymers, the Urbach edge position moved to shorter wavelengths, and the Urbach edge width became narrow. Teflon® ETFE shows an optical absorption edge at a wavelength of 314 nm and an Urbach edge width of 37 nm.

The optical absorbance of Teflon® FEP, Teflon® PFA, and Teflon® ETFE for Urbach edge analysis was determined by measuring the transmission of fluoropolymers films using the center mount technique. Tedlar® PVF UT20BG3 shows an optical absorption edge at a wavelength of 454 nm and an Urbach edge width of 17 nm, while Tedlar® PVF TR10AH9 shows an optical absorption edge at a wavelength of 318 nm and an Urbach edge width of 11 nm (Fig. 9). The Urbach fitting range wavelength of the materials of interest is summarized in Table 3.

4.2. Ethylene backbone polymers (EBP)

Ethylene backbone polymers such as the ethylene copolymers with vinyl acetate are widely used as encapsulants in PV. As
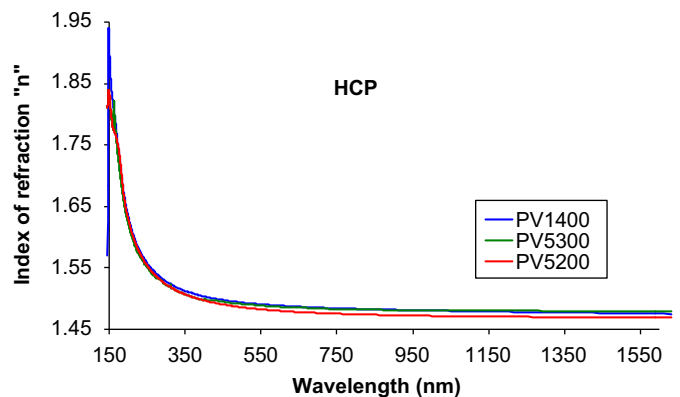

Fig. 10. Index of refraction, *n*, determined from ellipsometric data for ethylene backbone polymers.

indicated in NREL studies of ethylene backbone based encapsulants, ethylene-based ionomers showed superior performance after 4000 h of exposure to 42 UV suns [53].

4.2.1. Index of refraction

The index of refraction versus wavelength of ethylene backbone polymers is shown in Fig. 10. All of the EBP have a very similar index over the wavelength range measured. PV1400, a copolymer of ethylene and vinyl acetate commonly used in encapsulant formulations for flat plate c-Si PV, shows a slightly higher index than PV5200 and PV5300 polymers. DuPont™ PV5200, a polyvinylbutyral commonly used in thin-film PV, has the lowest index of refraction.

4.2.2. A/cm and haze

The absorption and haze of the ethylene backbone polymer samples are shown in Figs. 11 and 12. Elvax® PV1400 is an unformulated ethylene-vinyl acetate resin. It does not contain any UV stabilizing additives and therefore shows a shorter wavelength absorption edge than the DuPont™ PV5200 PVB and DuPont™ PV5300 ionomer encapsulants, which are fully formulated products. In addition, Elvax® PV1400 and DuPont™ PV5200 PVB exhibit some haze at these film thicknesses. DuPont™ PV5300 ionomer films are very clear and have the lowest haze of all the encapsulant polymers studied here.

4.2.3. Urbach edge analysis

In the Urbach analysis of the absorbance (A), Elvax® PV1400 shows the shortest optical absorption edge wavelength at 270 nm

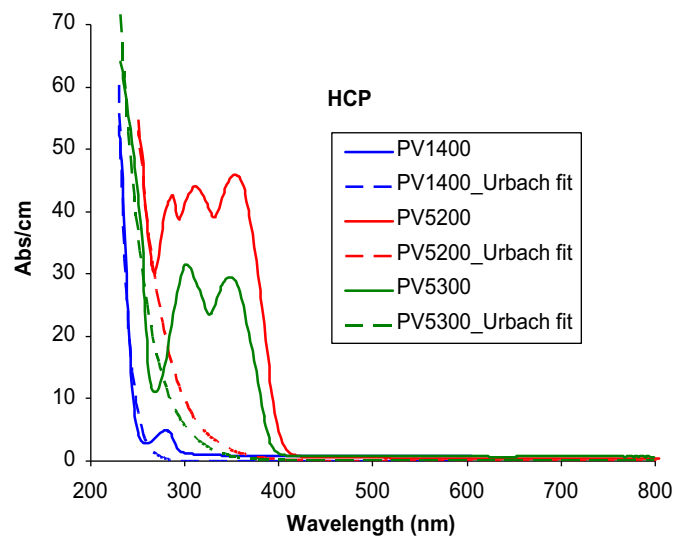and the narrowest Urbach edge width at 10 nm. DuPont™ PV5200 PVB shows a slightly longer optical absorption edge at a wavelength of 366 nm and a slightly wider Urbach edge width of 29 nm, while DuPont™ PV5300 ionomer shows an optical absorption edge at a wavelength of 346 nm and an Urbach edge width of 27 nm (Fig. 11).

4.3. Polyimides (PI)

Polyimides are most commonly used behind PV cells for thermal management and other purposes, and are therefore screened from direct sunlight. However, their optical properties are still of interest for potential applications in the PV industry.

4.3.1. Index of refraction

Fig. 13 shows the index of refraction versus wavelength for three different polyimides. As expected of polymers with an aromatic backbone, the index of refraction is much higher than that of the other polymers in this study. Kapton® E shows the highest index refraction of all polyimides.

Here we observe both normal dispersion (index increases with decrease in wavelength) and also anomalous dispersion [44] where, for wavelengths of light that are shorter than the fundamental absorption edge of the material, the index is seen to decrease with decrease in wavelength.
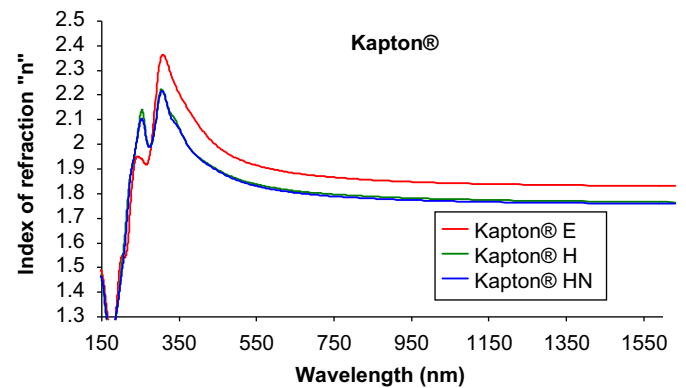

Fig. 11. Optical absorbance of ethylene backbone polymers.

Fig. 13. Index of refraction, n, determined from ellipsometric data for polyimides.

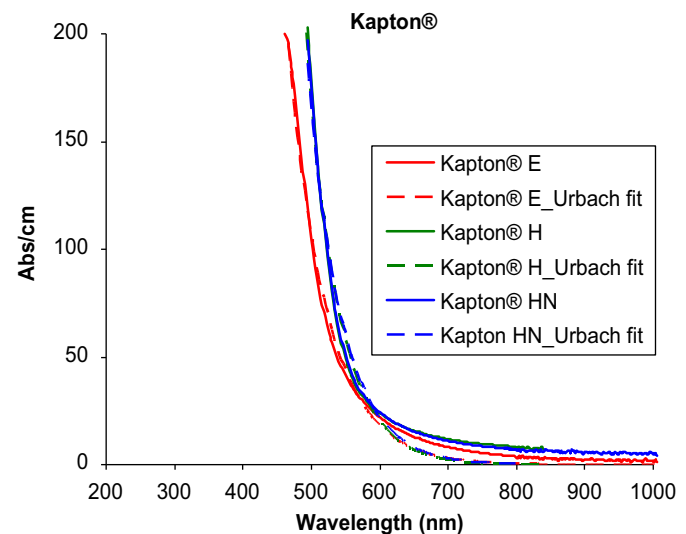

Fig. 12. Haze of ethylene backbone polymer films.
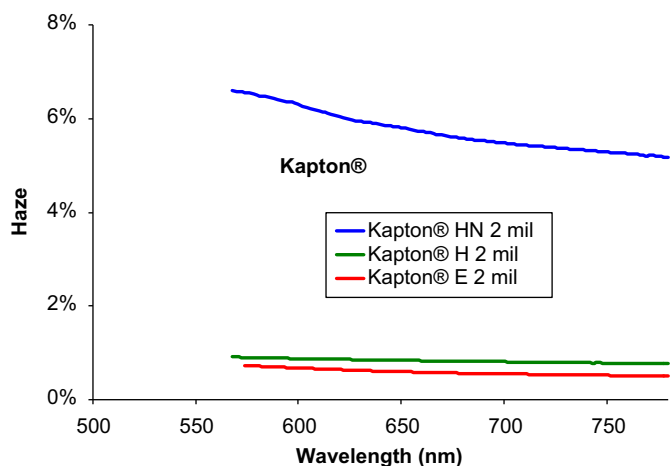

Fig. 14. Optical absorbance of polyimides.

Fig. 15. Haze of polyimide films.

4.3.2. A/cm and haze

The A/cm and haze of the polyimide polymers are shown in Figs. 14 and 15. The fundamental absorption edge of Kapton® H, Kapton® HN, and Kapton® E are at similar wavelengths, and can be associated with the visual yellow color of these materials. The higher haze in the Kapton® HN can be associated with additives. Polyimides start absorbing at ~550 or 600 nm and absorb highly below 500 nm. The haze goes to 100% below 500 nm, but the transmission goes to zero. The meaning of 100% haze in an opaque material is not sensible, when there is no transmission. The ASTM method says haze is only defined in spectral regions where the material is transparent. In the UV we say that haze values at wavelengths shorter than the onset of the UV absorption edge are not meaningful (the increase in haze as absorption increases, is not representative of a change in the source of the haze, it is an artifact of the drop in transmission), so we truncate the haze at the onset of the absorption edge. We also tend to think of the haze as a spectral property versus wavelength, and only give that average haze from 380 to 780 nm in a table, and if a material has its average haze number taken over a different range, we report the narrower range. The same arguments would apply in the infrared.

4.3.3. Urbach edge analysis

In the Urbach analysis of the absorbance (A), Kapton® E shows a longer optical absorption edge (763 nm) and a wider Urbach edge width (56 nm) than other two polyimides. Kapton® H shows an optical absorption edge at a wavelength of 741 nm and an Urbach edge width of 47 nm, while Kapton® HN shows an optical absorption edge at a wavelength of 731 nm and an Urbach edge width of 45 nm (Fig. 14).

5. Conclusions

Three groups of polymers encompassing ten materials have been studied using ellipsometry and transmission measurements to determine their optical properties. These materials have differing compositions and additives, which give rise to systematic changes in the optical properties such as the index of refraction and optical absorbance. The unique optical properties of these materials make them suitable for various applications in the photovoltaic industry.

References

[1] Roger H. French, Hoang V. Tran, Immersion lithography: photomask and wafer-level materials, Annual Review of Materials Research 39 (2009) 93–126.
[2] Richard M. Swanson, Photovoltaic concentrators, in: Antonio Luque, Steven Hegedus (Eds.), Handbook of Photovoltaic Science and Engineering, John Wiley, Hoboken NJ, 2003, pp. 449–503 (Chapter 11).
[3] R.H. French, J.M. Rodriguez-Parada, M.K. Yang, M.F. Lemon, E.C. Romano, P. Boydell, materials for concentrator photovoltaic systems: optical properties & solar radiation durability, in: Proceedings of the CPV-6 Conference, vol. 1277, Freiburg, Germany, 2010, pp. 127–130.
[4] J. Chaves, Introduction to Nonimaging Optics, CRC Press, Taylor & Francis Group, Florida, 2008.
[5] S.Hunter Richard, The Measurement of Appearance, John Wiley & Sons, 1987.
[6] G. Jorgensen, C. Kennedy, D. King, K. Terwilliger, Optical Durability Testing of Candidate Solar Mirrors", NREL/TP-520-28110, available at: ⟨http://www.nrel.gov/docs/fy00osti/28110.pdf⟩, March 2000.
[7] M.K. Yang, R.H. French, E.W. Tokarsky, Journal of Micro/Nanolithography, MEMS and MOEMS 7 (3) (2008) 1–9 033010.
[8] R.H. French, R.C. Wheland, W. Qiu, M.F. Lemon, E. Zhang, J. Gordon, V.A. Petrov, V.F. Cherstkov, N.I. Delaygina, Journal of Fluorine Chemistry 122 (2003) 63–80.
[9] G.L. Tan, M.F. Lemon, R.H. French, D.J. Jones, Optical properties and London dispersion forces of amorphous and crystalline silica determined by vacuum ultraviolet spectroscopy and spectroscopy ellipsometry, Physical Review B 72 (205117) (2005) 1–10.
[10] R.H. French, H. Müllejans, D.J. Jones, Optical properties of aluminum oxide: determined from vacuum ultraviolet and electron energy loss spectroscopies, Journal of the American Ceramic Society 81 (10) (1998) 2549–2557.
[11] K. van Benthem, G. Tan, R.H. French, L.K. Denoyer, R. Podgornik, V.A. Parsegian, Graded interface models for more accurate determination of van der-waals – london dispersion interactions across grain boundaries, Physical Review B 74 (205110) (2006) 1–12.
[12] R.H. French, D.J. Jones, H. Müllejans, S. Loughin, A.D. Dorneich, P.F. Carcia, Optical properties of aluminum nitride: determined from vacuum ultraviolet spectroscopy and spectroscopic ellipsometry, Journal of Materials Research, 14, 4337–4344 (1999).
[13] R. Rajter, R. Podgornik, V.A. Parsegian, R.H. French, W.Y. Ching, van der Waals–London dispersion interactions for optically anisotropic cylinders: metallic and semiconducting single wall carbon nanotubes, Physical Review B. 76 (045417) (2007).
[14] R. Rajter, R.H. French, van der Waals–London Dispersion Interaction Framework for Experimentally Realistic Carbon Nanotube Systems, Int. J. Mat. Res. 101 (1) (2010) 27–42.
[15] R.H. French, K.I. Winey, M.K. Yang, W. Qiu, Australian, "optical properties, electronic structure and dispersion interactions of polystyrene, Australian Journal of Chemistry 60 (2007) 251–263.
[16] R.H. French, J.S. Meth, J.R.G. Thorne, R.M. Hochstrasser, R.D. Miller, Synthetic Metals 50 (1-3) (1992) 499–508.
[17] G.Y.N. Chan, T.C. Hughes, K.M. McLean, G.A. McFarland, X. Nguyen, J.S. Wilkie, G. Johnson, Biomaterials 27 (8) (2006) 1287–1295.
[18] W. Jang, H.S. Lee, S. Lee, S. Choi, D. Shin, H. Han, Materials Chemistry and Physics 104 (2007) 342–349.
[19] K. Seki, H. Tanaka, T. Ohta, Y. Aoki, A. Imamura, H. Fujimoto, H. Yamamoto, H. Inokuchi., Physica Scripta 41 (1990) 167.
[20] A.E. Stiegman, D.E. Brinza, M.S. Anderson, T.K. Minton, E.G. Laue, R.H. Liang, An Investigation of the Degradation of Fluorinated Ethylene Propylene (FEP) Copolymer Thermal Blanket Materials Aboard LDEF and in the Laboratory, JPL Publication, May 1991, pp. 91–100.
[21] Dennis A. Russell, Larry B. Fogdall, Gail Bohnhoff-Hlavacek, Simulated Space Environmental Testing of Thin Films, Boeing Report to NASA Langley Research Center (Contract No. L-9162), November 1999.
[22] Kenneth K.S. Lau, Jeffrey A. Caulfield, Karen K. Gleason, Variable angle spectroscopic ellipsometry of fluorocarbon films from hot filament chemical vapor deposition, Journal of Vacuum Science and Technology A 18 (2000) 2404. doi:10.1116/1.1288191.
[23] D.J. Shelton, J.S. Tharp, G. Zummo, W.R. Folks, G.D. Boreman, Fabrication of Periodic Microstructures on Flexible Polyimide Membranes, College of Optics and Photonics/CREOL, University of Central Florida, Orlando, Florida 32816–2700.
[24] W.R. Folks, J. Ginn, D. Shelton, J. Tharp, G. Boreman. Spectroscopic Ellipsometry of Materials for Infrared Micro-Device Fabrication, College of Optics &

Photonics, CREOL & FPCE, University of Central Florida, Orlando, Florida, 32816-2700, USA.

[25] G. Kecskemeti, T. Smausz, N. Kresz, Zs. Toth, B. Hopp, D. Chrisey, O. Berkesi, Pulsed laser deposition of polyhydroxybutyrate biodegradable polymer thin films using ArF excimer laser, Applied Surface Science 253 (3) (2006) 1185–1189. doi:10.1016/j.apsusc.2006.01.084.

[26] W. Folks, S. Pandey, G. Pribil, D. Slafer, M. Manning, G. Boreman, Reflective infrared ellipsometry of plastic films, International Journal of Infrared and Millimeter Waves 27 (2006) 1553–1571.

[27] G.M. Wallner, W. Platzer, R.W. lang, Structure-property correlations of polymeric films for transparent insulation wall applications. Part1: solar optical properties, Solar Energy 79 (2005) 593–602.

[28] G.M. Wallner, W. Platzer, R.W. Lang, Structure-property correlations of polymeric films for transparent insulation wall applications. Part2: infrared optical properties, Solar Energy 79 (2005) 583–592.

[29] G. Oreski, D.T. Scharnuter, G.M. Wallner, Determination of optical properties of transparent polymer film using UV/vis spectroscopy, Solar Energy Materials & Solar Cell 94 (2010) 884–891.

[30] G.M. Wallner, C. Weigl, R.W. Lang, Polymer films for solar energy applications—thermoanalytical and mechanical characterization of ageing behavior, polymer Degradation and Stability 85 (2004) 1065–1070.

[31] G.M. Wallner, R.W. Lang, aging of polymeric films for transparent insulation wall applications, Solar Energy 79 (2005) 603–611.

[32] M. DeBergalis, Journal of Fluorine Chemistry 125 (2004) 1255–1257.

[33] H.G. Tompkins, Handbook of Ellipsometry, William Andrew, Inc, New York, 2005, pp. 569–636.

[34] H.G. Tompkins, W.A. McGahan, Spectroscopic Ellipsometry and Reflectometry, Wiley, New York, 1999.

[35] H.G. Tompkins, A. User's, Guider to Ellipsometry, Academic press, Boston, 1993.

[36] J. A. Woollam Co. Inc., 645 M Street, Suite 102, Lincoln, NE 68508 USA. ⟨available at http://dmseg5.case.edu/Groups/French/download/0208fwootenopticalpropertiesofsolids.pdf⟩.

[37] B. Johs, R.H. French, F.D. Kalk, W.A. McGahan, J.A. Woollam, Optical interference coatings,, SPIE 2253 (1098) (1994).

[38] J.A. Woollam, B. Johs, C.M. Herzinger, J. Hilfiker, R. Synowicki, C.L. Bungay, Overview of variable angle spectroscopic ellipsometry (VASE), part I: basic theory and typical applications", SPIE CR72 (1999) 3–28.

[39] M.E. Innocenzi, R.T. Swimm, M. Bass, R.H. French, M.R. Kokta, Optical absorption in undoped yttrium aluminum garnet, Journal of Applied Physics 68 (3) (1990) 1200–1204.

[40] M.E. Innocenzi, R.T. Swimm, M. Bass, R.H. French, A.B. Villaverde, M.R. Kokta, Room temperature optical absorption in undoped IIs-Al2O3, Journal of Applied Physics 67 (12) (1990) 7542–7546.

[41] J.A. Woollam, B. Johs, C.M. Herzinger, J. Hilfiker, R. Synowicki, C.L. Bungay, Overview of variable angle spectroscopic ellipsometry (VASE), part II: advanced applications, SPIE CR72 (1999) 29–58.

[42] Caulfield and Gleason Lau, Journal of Vacuum Science andTechnology A 18 (5) (2000) 2404–2411 Sep/Oct.

[43] Varian Cary Division, Palo Alto CA, 94303.

[44] R.H. French, H. Sewell, M.K. Yang, S. Peng, D. McCafferty, W. Qiu, R.C. Wheland, M.F. Lemon, L. Markoya, M.K. Crawford, Imaging Of 32-nm 1:1 lines and spaces using 193 nm immersion interference lithography with second-generation immersion fluids to achieve a numerical aperture Of 1.5 and a k1 Of 0.25, Journal of Microlithography, Microfabrication and Microsystems, Topical Issue on Hyper-NA Imaging 4 (3) (2005) 031103.

[45] Stuart White, Evaluation of the Cary Absolute Specular Reflectance Accessory for the measurement of Optical Constants of Thin Film, Varian, UV-45, June 1988.

[46] F. Urbach, The long-wavelength edge of photographic sensitivity and of the electronic absorption of solids, Physical Review 92 (1324) (1953).

[47] F. Wooten, Optical Properties of Solids, Academic Press, 1972.

[48] D.C. Miller, M.D. Kempe, C.E. Kennedy, S.R. Kurtz, Analysis of transmitted optical spectrum enabling accelerated testing of CPV design, in: Proceedings of the SPIE Optics and Photonics 2009 Conference.

[49] IUPAC Handbook Definition. ⟨http://www.iupac.org/goldbook/A00035.pdf⟩.

[50] H.R. Philipp, in: E.D. Palik (Ed.), Handbook of Optical Constants of Solids, vol. I, Academic, New York, 1985, p. 753.

[51] M. DeBergalis, Fluoropolymer films in the photovoltaic industry, in: Proceedings of Fluorine in Alternative Energy Sources Symposium, Journal of Fluorine Chemistry, vol. 125 (8), August 2004, pp 1255–1257, 0022-1139, 10.1016/j.jfluchem.2004.05.013.

[52] G. Jorgensen, C. Kennedy, D. King, Optical Durability testing of Candidates Solar mirrors, NREL/TP-520-28110, March 2000.

[53] M. Kempe, T. Moricone, M. Kilkenny, J. Zhang Accelerated stress testing of hydrocarbon based encapsulants for medium-concentration CPV applications, in: Proceedings of the 34th IEEE PVSC, Philadelphia, PA, June 7, 2009.